Journal of Inorganic and General Chemistry
ZAAC
Zeitschrift für anorganische und allgemeine Chemie
DOI: 10.1002/zaac.202100143
ARTICLE

Broadband impedance spectroscopy of $Li_4Ti_5O_{12}$: from nearly constant loss effects to long-range ion dynamics

Bernhard Gadermaier,*[a] Katharina Hogrefe,[a] Paul Heitjans,[b] and H. Martin R. Wilkening*[a]

Dedicated to the 60th birthday of Professor Dr. Josef Breu

$Li_4Ti_5O_{12}$ (LTO) is known as one of the most robust and long-lasting anode materials in lithium-ion batteries. As yet, the Li-ion transport properties of LTO are, however, not completely understood. Here, we used broadband impedance spectroscopy spanning a wide temperature range to investigate the full electrical response of LTO over a wide frequency range. It turned out that the isotherms recorded entail information about two relaxation processes. While at high temperatures the isotherms show a frequency independent plateau that corresponds to poor long-range ion transport ($<10^{-11}$ S cm^{-1} (298 K), 0.79 eV), they reveal a second region, seen at lower temperatures and higher frequencies, which we attribute to short-range ion dynamics (10^{-8} S cm^{-1}) with a significantly reduced activation energy of ca. 0.51 eV. At even lower temperatures, the isotherms are fully governed by nearly constant loss behavior, which has frequently been explained by cage-like dynamics. The present results agree with those earlier presented by ^{7}Li NMR spin-lattice relaxation measurements being sensitive to dynamic processes taking place on quite different length scales. Our findings unveil complex Li^+ ion dynamics in LTO and help understand its superior electrochemical properties.

Introduction

Studying the principles that govern the irregular movements of small cations such as H^+ and Li^+ in solids belongs to the traditional research themes in solid-state physical chemistry. Analyzing the diffusion properties of materials providing various structural motifs will help us to develop materials with tailored diffusion properties.

Even until now, we do only partly understand the relevant diffusion mechanisms[1] in site-disordered materials usually providing a range of energetically possible diffusion pathways.[2] Such an understanding, also including the important role of structural disorder and defects,[3] is, however, urgently needed if we want to develop active materials for, *e.g.*, energy storage systems[4] that rely on both sufficiently high ionic[5] and electronic conduction.[6]

Here, $Li_4Ti_5O_{12}$ (LTO, space group *Fd*-3 *m*) served as a model system,[3c,7] inspired by applications as anode material,[8] to investigate long-range as well as short-range Li^+ ion dynamics within a spinel-type structure.[9] Long-range ion transport and short-range Li^+ translational motions are expected to manifest themselves in characteristic features of the corresponding broadband conductivity isotherms,[3b,10] which we recorded over a wide temperature (and frequency) range.

In LTO the Li ions occupy the two inequivalent sites *viz* the sites 8*a* and 16*d*, see Figure 1. Stoichiometric LTO is a rather poor ionic (and electronic, $<10^{-13}$ S cm^{-1})[7b,11] conductor at room temperature[9b] which shows an overall (direct current, DC) conductivity of $<10^{-11}$ S cm^{-1} at 298 K. This value corresponds to the prominent DC plateau which determines the conductivity isotherms at elevated temperatures.[9b] The present study is aimed at answering the question whether other processes do also contribute to the full electric response.[12] In fact, depending on frequency and temperature, another electric process comes into play that might be attributed to the faster 8*a*–16*c* exchange process.[9a,13] Such (local) translational dynamics are indeed supposed to govern 3D Li^+ ion dynamics in $Li_{4+x}Ti_5O_{12}$ with $x>0$, which is formed during the charging process in Li-ion full cells.[9a,13–14]

Results and Discussion

Figure 2 shows the broadband dielectric response that is obtained if a dense pellet of polycrystalline LTO is subjected to an alternating voltage of 100 mV_{rms}. While in Figure 2a the real part of the conductivity σ' is plotted at fixed frequency for

[a] Dr. B. Gadermaier, K. Hogrefe, Prof. Dr. H. M. R. Wilkening
Institute for Chemistry and Technology of Materials
Graz University of Technology
Stremayrgasse 9
8010 Graz, Austria
E-mail: wilkening@tugraz.at
bernhard.gadermaier@tugraz.at
[b] Prof. Dr. P. Heitjans
Institute of Physical Chemistry and Electrochemistry
Leibniz Universität Hannover
Callinstraße 3–3a
30167 Hannover, Germany

Supporting information for this article is available on the WWW under https://doi.org/10.1002/zaac.202100143

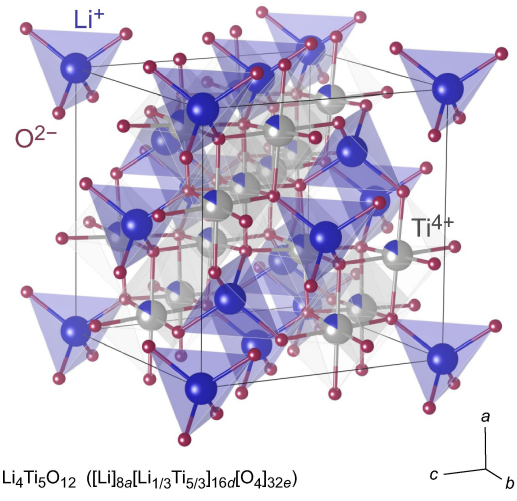

Figure 1. Crystal structure of $Li_4Ti_5O_{12}$ (*Fd*-3 *m*). The tetrahedral voids 8*a* are fully occupied by Li^+ ions; the sites 16*d* are randomly occupied by both Li^+ (1/3) and Ti^{4+} (5/3). Two tetrahedral 8*a* sites are directly connected by an empty octahedral void (16*c*) by sharing common faces, not shown.

various temperatures *T*, Figure 2b shows the corresponding conductivity isotherms $\sigma'(\nu)$.

The isotherms shown in Figure 2b reveal that the total conductivity passes through two distinct, frequency-independent plateau regions; this feature is especially seen if we consider the isotherm recorded at $T = 90\,^{\circ}C$. At even higher *T*, polarization effects appear due to fast Li ion transport and piling up of the charge carriers in front of the ion-blocking electrodes used to measure the spectra, see the arrow pointing to this region seen at 210 °C. At low frequencies the DC plateau is seen that corresponds to long-range, through-going ionic transport. At room temperature σ_{DC} amounts to values in the order of $10^{-11}\,S\,cm^{-1}$ (Figure 2b) clearly showing the poor transport characteristics of LTO. This response is associated with capacitance values in the pF regime,[15] hence it indeed refers to a bulk process and does not mirror the effect of ion-blocking grain boundaries. The latter might block long-range ion transport, as has been shown for many oxide-type materials or silicates.[16]

When going to higher frequencies a second plateau is passed through. Its DC conductivity is higher by ca. 3 orders of magnitude. Again, the associated capacitance *C* is in the order of some pF reflecting another bulk response, which, most likely, proceeds on a shorter length scale. The corresponding electric modulus spectra are shown in the insets of Figure 2a and 2b. As the amplitude of $M''(\nu)$ is proportional to $1/C$,[15] the difference in capacitance of the two electric relaxation processes turned out to be rather small; the amplitudes differ from each other only by a factor of 2.6. The distance of the two modulus peaks on the frequency scale seen in the insets of Figure 2 agree with the ratio of the conductivities of the two plateau regions.

If we cool the pellets further down, we see that at −100 °C the isotherms do follow an almost linear behavior, $\sigma'(\nu) \propto \nu^p$ ($p = 1$), that is fully developed at $T = -160\,^{\circ}C$. The linear

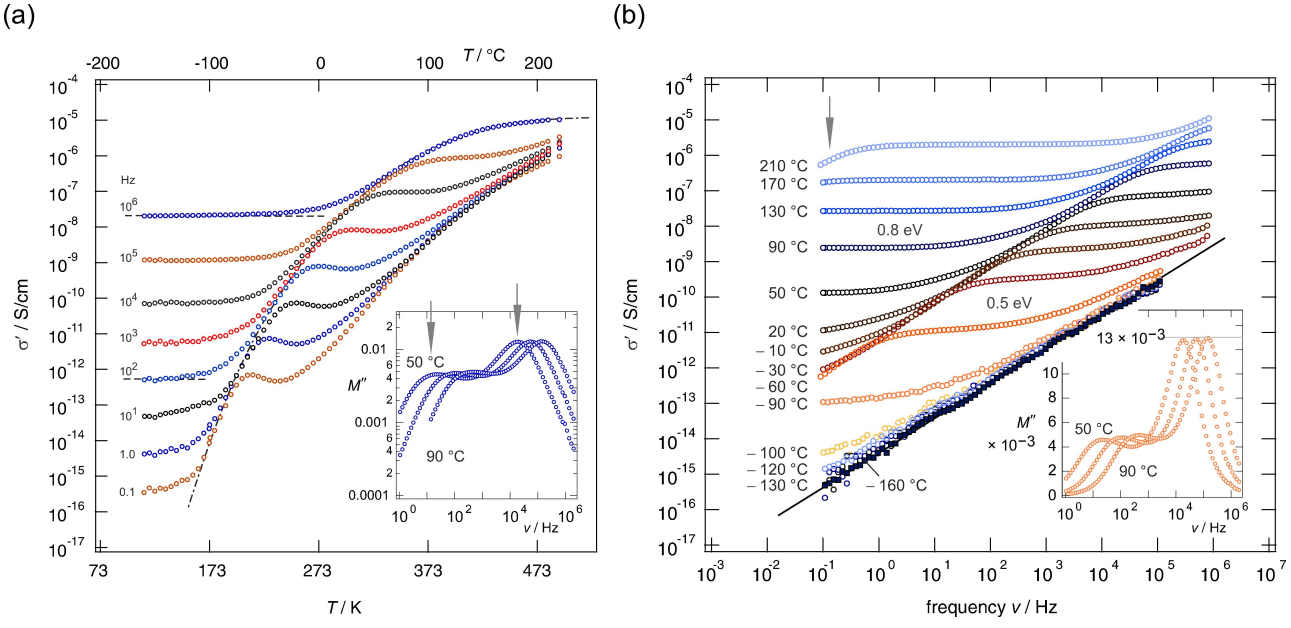

Figure 2. (a) Change of the real part, σ', of the complex conductivity as a function of temperature *T* for fixed frequency; curves were recorded under N_2 atmosphere (drying at 100 °C (30 min), cooling down to −130 °C then heating up to 210 °C). Dashed lines are to guide the eye. The inset, a logarithmic plot, displays the modulus curves $M''(\nu)$ selected for three temperatures: 50 °C, 70 °C and 90 °C. (b) $\sigma'(\nu)$ isotherms recorded over a frequency range of 7 orders of magnitude revealing NCL behaviour at low *T* and two distinct DC plateaus, which are best seen for the curves at 90 °C. The straight line shows the linear dependence of σ' on frequency. The inset shows M'' *vs* ν using a logarithmic plot. The two amplitudes of the electric modulus do only differ by a factor of 2.6 and, thus, point to two bulk processes sensed.

dependence of σ' on frequency is known as the so-called nearly constant loss (NCL)[17] behavior as it corresponds to an almost constant imaginary part, ε'', of the complex (relative) permittivity. Indeed, in Figure 3a, which shows the change of ε'' as a function of frequency but for different temperatures, $\varepsilon''(\nu)$ recorded at −160 °C turned out to be almost independent of temperature; this temperature independence is also seen for σ' if we regard the low temperatures and high frequencies, see Figure 2b. NCL behavior is frequently associated with cage-like ion dynamics that is, for example, present in the famous silver-ion conductor $RbAg_4I_5$ with its pocket-like cages[17d] that leave behind the typical NCL response for strictly localized ion dynamics, which does not contribute to long-range ion transport. This feature belongs to one of the universal responses in conductivity spectroscopy.[17c,f] It is usually seen in glassy materials,[17b,e,18] but is also present in some crystalline materials.[17d,19] LTO is another crystalline model system that shows this feature. A Li ion conductor where NCL behavior was observed both in the glassy and crystalline form with the same chemical compositions is $LiAlSi_2O_6$.[20]

Analyzing the temperature dependence of the DC conductivities associated with the two plateau regions seen in Figure 2b, we obtain Arrhenius behavior; the Arrhenius diagram is constructed by plotting $\sigma_{DC}T$ as a function of the inverse temperature, 1000/T, see Figure 3b. The first plateau seen at low frequencies yields an activation energy of 0.79 eV. This value excellently agrees with that[9b] which was deduced from ^{7}Li spin-alignment echo (SAE) NMR being a method that is sensitive to slow, long-range ion dynamics.[21] Similar to σ_{DC}, SAE samples successful ion displacements in the bulk that are characterized by a change of the electric quadrupole frequency. SAE NMR is able to directly record a single particle (or single spin) motional correlation function.[21–22] Most likely, SAE NMR and σ_{DC} probe slow ion exchange processes involving all of the Li ions in LTO including the less mobile ones residing on the 16*d* sites.[9b] Recently, their low mobility was revealed by 2D exchange NMR spectroscopy.[13]

The second plateau reveals an activation of only 0.51 eV and points to a more locally restricted diffusion process, see Figure 3b. Indications of such a process are also given by earlier ^{7}Li NMR spin-lattice relaxation measurements pointing to activation energies in the order of 0.25 eV.[9b] We think that this process seen here reflects localized (forward-backward) 8*a*–16*c* jumps between the neighboring tetrahedra and octahedra that share common faces. This diffusion process is essential for $Li_{4+x}Ti_5O_{12}$ with $x>0$, as for such compositions the 16*c* sites get filled with Li^+ ions.[23] Simultaneously, to reduce the ion-ion Coulomb interactions, Li ions escape from the originally fully occupied 8*a* sites and occupy the 16*c* sites.[9a,13] However, the simultaneous occupation[23] of the neighboring sites 16*c* and 8*a* results in a frustrated geometry for the Li^+ ions that is the origin for rapid Li^+ exchange in Li-inserted $Li_{4+x}Ti_5O_{12}$,[9a] as also suggested by Wagemaker *et al.*,[9h] Pang *et al.*[24] and Zhang *et al.*[9c] Other studies considered the involvement of 32*e* split sites[25] as well as occupational disorder, that is, the participation of anti-site defects assisting in Li ion diffusion.[12] In contrast to Ren *et al.* we do only observe two relaxation processes in our LTO sample.[25c] Pang *et al.* [24] pointed out that the 32*e* sites[25a] may act as a bridge connecting the 8*a* and 16*c* sites linearly.

Our interpretation that the two DC plateau regions, as well as the two modulus peaks, have to be ascribed to two bulk processes, is further corroborated by measurements of the real part of the electric permittivity shown in Figure 3c. Values in the low frequency regions clearly indicate bulk dielectric processes. Hence, LTO is one of the very rare materials where two dynamic processes can be differentiated by conductivity spectroscopy. An early other example was β-$LiAlSiO_4$ (β-eucryptite).[26] Most likely, the behaviour of LTO is caused by the 16*d* ions having only access to slow diffusion pathways, whereas the 8*a* ions can locally jump between the filled 8*a* sites and the empty 16*c* sites.

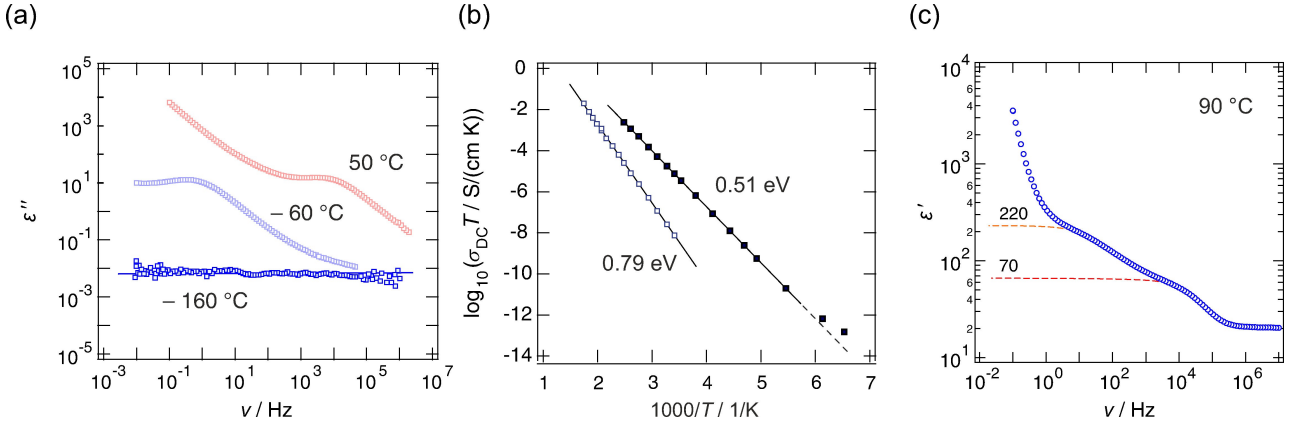

Figure 3. (a) Permittivity isotherms that reveal NCL behaviour at the lowest temperatures, which shows an almost frequency independent imaginary part, ε'', of the complex permittivity. (b) Arrhenius plot of the DC conductivities (plotted as $\sigma_{DC}T$ *vs* 1/T) extracted from the frequency independent plateau regions of the conductivity isotherms shown in Figure 2b. Values indicate activation energies. (c) Change of the real part of the dielectric permittivity as a function of frequency. The two responses point to ε' values of 70 and 220. See text for further explanation.

The present findings do also shed light on the complex results obtained by Fehr *et al.* who studied $Li_4Ti_5O_{12}$ under different conditions[7a] thereby revealing changes of the overall conductivity with atmosphere and during several heating and cooling runs. We anticipate that the defect chemistry depending on the oxygen partial pressure will affect the results. Future studies shall, however, consider the fact that, below 500 K, two dielectric processes are at play in stoichiometric LTO, which, most likely, reflect two distinct dynamic Li^+ processes with activation energies of approximately 0.8 eV and 0.5 eV, respectively.

Conclusions

$Li_{4+x}Ti_5O_{12}$ is known as a powerful anode material that offers fast Li^+ diffusion and efficient electron transport if additional Li (Li^+ and e^-) is chemically or electrochemically inserted. The compound with $x=0$ is, however, a rather poor ionic conductor governed by a relatively high activation energy of ca. 0.8 eV. Here, besides the main DC plateau dominating the conductivity spectra at elevated temperatures, broadband conductivity spectroscopy reveals a second electrical response that points to enhanced bulk diffusivity that is characterized by an activation energy of only approximately 0.5 eV. The same response is also seen in electric modulus spectroscopy and permittivity studies. It is ascribed to short-range (forward-backward) Li^+ translational dynamics that do not contribute to long-range ion dynamics. Most likely, this process becomes the dominant one upon lithiation of LTO. In the low temperature region, LTO reveals the classical NCL-type behavior pointing to dynamic processes being spatially restricted even more than those thermally activated by 0.5 eV.

Experimental Section

LTO was purchased from SüdChemie. The same sample was used in earlier NMR studies to investigate Li^+ ion diffusivity. For the impedance measurements the as-received polycrystalline powder samples were pressed to cylindrical pellets with a diameter of 8 mm and a thickness of 0.5 mm. Gold electrodes, blocking any Li^+ ion transport, were sputtered on both sides (Leica, EM SCD050) to ensure electrical contact.

Alternating current (AC) impedance data (0.1 Hz up to 10^7 Hz) were recorded with a Novocontrol Concept 80 spectrometer in combination with an active BDS 1200 cell and a ZGS interface (Novocontrol). A QUATRO cryo-system was employed to precisely control and monitor the temperature via Pt100 thermocouples. Here, we varied the temperature T from −160 °C to 210 °C. Data were analyzed with the software IGOR Pro developed by WaveMetrics. The crystal structure was drawn with the help of the VESTA software package.[27]

Acknowledgements

We thank the Deutsche Forschungsgemeinschaft (DFG) for financial support in the frame of the former research unit FOR 1277 (2010–2017) "Mobilität von Lithiumionen in Festkörpern (molife)" (WI 3600 2-1). Furthermore, financial support by the FFG project safe battery is gratefully acknowledged. P.H. is grateful to the State of Lower Saxony (Germany) for the Niedersachsen Professorship "Mobility of Ions in Solids".

Conflict of Interest

The authors declare no conflict of interest.

Keywords: LTO · anode materials · conductivity · Li diffusion · dielectric properties

[1] a) S. Hull, *Rep. Prog. Phys.* **2004**, *67*, 1233–1314; b) J. Maier, *J. Electroceram.* **2015**, *34*, 69–73; c) P. Heitjans, S. Indris, *J. Phys. Condens. Matter* **2003**, *15*, R1257–R1289.

[2] a) I. Hanghofer, M. Brinek, S. L. Eisbacher, B. Bitschnau, M. Volck, V. Hennige, I. Hanzu, D. Rettenwander, H. M. R. Wilkening, *Phys. Chem. Chem. Phys.* **2019**, *21*, 8489–8507; b) M. Brinek, C. Hiebl, K. Hogrefe, I. Hanghofer, H. M. R. Wilkening, *J. Phys. Chem. C* **2020**, *124*, 22934–22940.

[3] a) B. Gadermaier, L. Resch, D. M. Pickup, I. Hanghofer, I. Hanzu, P. Heitjans, W. Sprengel, R. Wurschum, A. V. Chadwick, H. M. R. Wilkening, *Solid State Ionics* **2020**, *352*; b) M. Wilkening, V. Epp, A. Feldhoff, P. Heitjans, *J. Phys. Chem. C* **2008**, *112*, 9291–9300; c) D. Prutsch, S. Breuer, M. Uitz, P. Bottke, J. Langer, S. Lunghammer, M. Philipp, P. Posch, V. Pregartner, B. Stanje, A. Dunst, D. Wohlmuth, H. Brandstätter, W. Schmidt, V. Epp, A. Chadwick, I. Hanzu, M. Wilkening, *Z. Phys. Chem.* **2017**, *231*, 1361–1405; d) D. Wohlmuth, V. Epp, P. Bottke, I. Hanzu, B. Bitschnau, I. Letofsky-Papst, M. Kriechbaum, H. Amenitsch, F. Hofer, M. Wilkening, *J. Mater. Chem. A* **2014**, *2*, 20295–20306; e) D. Wohlmuth, V. Epp, B. Stanje, A. M. Welsch, H. Behrens, M. Wilkening, *J. Am. Ceram. Soc.* **2016**, *99*, 1687–1693; f) P. Heitjans, M. Masoud, A. Feldhoff, M. Wilkening, *Faraday Discuss.* **2007**, *134*, 67–82.

[4] a) D. Larcher, J. M. Tarascon, *Nat. Chem.* **2015**, *7*, 19–29; b) J. M. Tarascon, *ChemSusChem* **2008**, *1*, 777–779.

[5] a) J. C. Bachman, S. Muy, A. Grimaud, H. H. Chang, N. Pour, S. F. Lux, O. Paschos, F. Maglia, S. Lupart, P. Lamp, L. Giordano, Y. Shao-Horn, *Chem. Rev.* **2016**, *116*, 140–162; b) Z. Z. Zhang, Y. J. Shao, B. Lotsch, Y. S. Hu, H. Li, J. Janek, L. F. Nazar, C. W. Nan, J. Maier, M. Armand, L. Q. Chen, *Energy Environ. Sci.* **2018**, *11*, 1945–1976; c) V. Thangadurai, S. Narayanan, D. Pinzaru, *Chem. Soc. Rev.* **2014**, *43*, 4714–4727; d) M. Uitz, V. Epp, P. Bottke, M. Wilkening, *J. Electroceram.* **2017**, *38*, 142–156.

[6] a) M. S. Whittingham, *Chem. Rev.* **2004**, *104*, 4271–4301; b) J. B. Goodenough, Y. Kim, *Chem. Mater.* **2010**, *22*, 587–603.

[7] a) K. T. Fehr, M. Holzapfel, A. Laumann, E. Schmidbauer, *Solid State Ionics* **2010**, *181*, 1111–1118; b) C. H. Chen, J. T. Vaughey, A. N. Jansen, D. W. Dees, A. J. Kahaian, T. Goacher, M. M. Thackeray, *J. Electrochem. Soc.* **2001**, *148*, A102–A104; c) J. Wolfenstine, J. L. Allen, *J. Power Sources* **2008**, *180*, 582–585; d) L. Aldon, P. Kubiak, M. Womes, J. C. Jumas, J. Olivier-Fourcade, J. L. Tirado, J. I. Corredor, C. Pérez Vicente, *Chem. Mater.* **2004**, *16*, 5721–5725.

[8] E. Ferg, R. d Gummow, A. De Kock, M. Thackeray, *J. Electrochem. Soc.* **1994**, *141*, L147.

[9] a) W. Schmidt, P. Bottke, M. Sternad, P. Gollob, V. Hennige, M. Wilkening, *Chem. Mater.* **2015**, *27*, 1740–1750; b) M. Wilkening, R. Amade, W. Iwaniak, P. Heitjans, *Phys. Chem. Chem. Phys.* **2007**, *9*, 1239–1246; c) W. Zhang, D. H. Seo, T. Chen, L. J. Wu,

M. Topsakal, Y. M. Zhu, D. Y. Lu, G. Ceder, F. Wang, *Science* **2020**, *367*, 1030; d) A. Vasileiadis, N. J. J. de Klerk, R. B. Smith, S. Ganapathy, P. P. R. M. L. Harks, M. Z. Bazant, M. Wagemaker, *Adv. Funct. Mater.* **2018**, *28*; e) S. Ganapathy, A. Vasileiadis, J. R. Heringa, M. Wagemaker, *Adv. Energy Mater.* **2017**, *7*, 1601781; f) C. Wang, S. A. Wang, Y. B. He, L. K. Tang, C. P. Han, C. Yang, M. Wagemaker, B. H. Li, Q. H. Yang, J. K. Kim, F. Y. Kang, *Chem. Mater.* **2015**, *27*, 5647–5656; g) W. J. H. Borghols, M. Wagemaker, U. Lafont, E. M. Kelder, F. M. Mulder, *J. Am. Chem. Soc.* **2009**, *131*, 17786–17792; h) M. Wagemaker, E. R. H. van Eck, A. P. M. Kentgens, F. M. Mulder, *J. Phys. Chem. B* **2009**, *113*, 224–230; i) B. Ziebarth, M. Klinsmann, T. Eckl, C. Elsässer, *Phys. Rev. B* **2014**, *89*, 174301.

[10] F. Preishuber-Pflügl, P. Bottke, V. Pregartner, B. Bitschnau, M. Wilkening, *Phys. Chem. Chem. Phys.* **2014**, *16*, 9580–9590.

[11] H. Song, T.-G. Jeong, S.-W. Yun, E.-K. Lee, S.-A. Park, Y.-T. Kim, *Sci. Rep.* **2017**, *7*, 43335.

[12] H. H. Heenen, C. Scheurer, K. Reuter, *Nano Lett.* **2017**, *17*, 3884–3888.

[13] W. Schmidt, M. Wilkening, *J. Phys. Chem. C* **2016**, *120*, 11372–11381.

[14] a) M. Wilkening, W. Iwaniak, J. Heine, V. Epp, A. Kleinert, M. Behrens, G. Nuspl, W. Bensch, P. Heitjans, *Phys. Chem. Chem. Phys.* **2007**, *9*, 6199–6202; b) S. Ganapathy, M. Wagemaker, *Nat. Energy* **2020**, *5*, 424–425.

[15] J. T. S. Irvine, D. C. Sinclair, A. R. West, *Adv. Mater.* **1990**, *2*, 132–138.

[16] a) A. Kuhn, S. Narayanan, L. Spencer, G. Goward, V. Thangadurai, M. Wilkening, *Phys. Rev. B* **2011**, *83*, 094302; b) C. Hiebl, P. Loch, M. Brinek, M. Gombotz, B. Gadermaier, P. Heitjans, J. Breu, H. M. R. Wilkening, *Chem. Mater.* **2020**, *32*, 7445–7457.

[17] a) J. Habasaki, K. L. Ngai, *J. Phys. Chem. C* **2017**, *121*, 13729–13737; b) R. D. Banhatti, D. Laughman, L. Badr, K. Funke, *Solid State Ionics* **2011**, *192*, 70–75; c) K. Funke, R. D. Banhatti, C. Cramer, *Phys. Chem. Chem. Phys.* **2005**, *7*, 157–165; d) K. Funke, I. Ross, R. D. Banhatti, *Solid State Ionics* **2004**, *175*, 819–822; e) A. Rivera, A. Leon, C. P. E. Varsamis, G. D. Chryssikos, K. L. Ngai, C. M. Roland, L. J. Buckley, *Phys. Rev. Lett.* **2002**, *88*, 125902; f) C. Leon, A. Rivera, A. Varez, J. Sanz, J. Santamaria, C. T. Moynihan, K. L. Ngai, *J. Non-Cryst. Solids* **2002**, *305*, 88–95; g) C. Leon, A. Rivera, A. Varez, J. Sanz, J. Santamaria, K. L. Ngai, *Phys. Rev. Lett.* **2001**, *86*, 1279–1282.

[18] a) D. M. Laughman, R. D. Banhatti, K. Funke, *Phys. Chem. Chem. Phys.* **2010**, *12*, 14102–14108; b) D. M. Laughman, R. D. Banhatti, K. Funke, *Phys. Chem. Chem. Phys.* **2009**, *11*, 3158–3167; c) A. Rivera, J. Santamaria, C. Leon, J. Sanz, C. P. E. Varsamis, G. D. Chryssikos, K. L. Ngai, *J. Non-Cryst. Solids* **2002**, *307*, 1024–1030.

[19] a) A. Dunst, M. Sternad, M. Wilkening, *Mater. Sci. Eng. B* **2016**, *211*, 85–93; b) A. Rivera, C. Leon, J. Sanz, J. Santamaria, C. T. Moynihan, K. L. Ngai, *Phys. Rev. B* **2002**, *65*, 224302.

[20] A. K. Rizos, J. Alifragis, K. L. Ngai, P. Heitjans, *J. Chem. Phys.* **2001**, *114*, 931–934.

[21] M. Wilkening, P. Heitjans, *ChemPhysChem* **2012**, *13*, 53–65.

[22] M. Wilkening, P. Heitjans, *J. Phys. Condens. Matter* **2006**, *18*, 9849–9862.

[23] M. Wagemaker, D. R. Simon, E. M. Kelder, J. Schoonman, C. Ringpfeil, U. Haake, D. Lützenkirchen-Hecht, R. Frahm, F. M. Mulder, *Adv. Mater.* **2006**, *18*, 3169–3173.

[24] W. K. Pang, V. K. Peterson, N. Sharma, J.-J. Shiu, S.-h. Wu, *Chem. Mater.* **2014**, *26*, 2318–2326.

[25] a) A. Laumann, H. Boysen, M. Bremholm, K. T. Fehr, M. Hoelzel, M. Holzapfel, *Chem. Mater.* **2011**, *23*, 2753–2759; b) O. Dolotko, A. Senyshyn, M. J. Mühlbauer, H. Boysen, M. Monchak, H. Ehrenberg, *Solid State Sci.* **2014**, *36*, 101–106; c) S. Ren, J. Liu, D. Wang, J. Zhang, X. Ma, M. Knapp, L. Liu, H. Ehrenberg, *J. Alloys Compd.* **2019**, *793*, 678–685.

[26] B. Munro, M. Schrader, P. Heitjans, *Ber. Bunsenges. Phys. Chem.* **1992**, *96*, 1718–1723.

[27] K. Momma, F. Izumi, *J. Appl. Crystallogr.* **2008**, *41*, 653–658.

Manuscript received: April 21, 2021
Revised manuscript received: June 8, 2021
Accepted manuscript online: June 11, 2021